LA-UR-18-20101
Approved for public release; distribution is unlimited.

Title: (U) Influence of Compaction Model Form on Planar and Cylindrical Compaction Geometries

Author(s): Fredenburg, David A.
Carney, Theodore Clayton
Fichtl, Christopher Allen
Ramsey, Scott D.

Intended for: Report

Issued: 2018-01-05

(U) Influence of Compaction Model Form on Planar and Cylindrical Compaction Geometries

Compiled by:

D.A. Fredenburg, T.C. Carney, C.A. Fichtl, S.D. Ramsey
Los Alamos National Laboratory, Los Alamos NM, 87545
dafreden@lanl.gov

LA-UR-

UNCLASSIFIED

November 16, 2017

Preface

The dynamic compaction response of CeO_2 is examined within the frameworks of the Ramp and P-α compaction models. Hydrocode calculations simulating the dynamic response of CeO_2 at several distinct pressures within the compaction region are investigated in both planar and cylindrically convergent geometries. Findings suggest additional validation of the compaction models is warranted under complex loading configurations.

1 Introduction

The dynamic compaction of initially porous materials can be modeled in several ways using the LANL hydrocode FLAG,[1] where two of the more prevalent modeling choices are the Ramp and P-α models. In the simplest instance, the physical process of compaction (where voids are removed due to an applied load) is captured with a Ramp model. The Ramp model can be applied either as a single stage Ramp or a bi-linear Ramp. If the single stage Ramp is implemented with a small slope, this model represents a 'snow-plow' behavior,[2] where nearly any pressure $P > 0$ crushes out all of the porosity. At higher single stage slopes, and for bi-linear Ramps, the slopes of the Ramps are often set to reflect the dynamic compaction response measured from one-dimensional (1D) planar impact experiments. Computationally, the P-α model performs the same function as the Ramp; however, the physics underlying the P-α model are slightly more involved. In either case, the computationally obtained density ρ (or volume V) is used to calculate the pressure based on the parameters specified in the models.

In most instances, calibration for the Ramp and P-α models occurs by means of fitting 1D planar compaction data. However, in most real-world applications for granular compaction (meteoric or planetary impact, ballistic penetration, explosive mining operations, etc.) the impulse does not occur under 1D loading, but rather under more complex loading configurations. As such, the present work seeks to determine if the recently developed PHELIX platform[3] can provide experimental validation of the Ramp and P-α model implementations in FLAG under non-planar complex loading configurations. The relevant drives and geometries accessible by PHELIX were first investigated for granular SiO_2, but its relatively low crush pressure restricted the range of dynamic experiments that could be conducted on PHELIX for model validation. To access a broader range of compaction phenomena CeO_2, which has a relatively high crush pressure ($\sim$12 GPa for 55% theoretical density), was chosen for further examination.

This work investigates the simulated response of CeO_2 under both 1D planar and non-planar loading configurations to determine what, if any, differences in the calculated response may arise due to modeling compaction with the Ramp and P-α models in FLAG. As such, relevant details of the two compaction models are presented first, followed by corresponding model fits to available 1D planar compaction data for CeO_2. Next, the Hugoniot states calculated with both models are compared to experimental planar compaction data. Subsequently, a series of calculations exploring the shock/re-shock and shock/release states achieved in CeO_2 as a function of compaction model choice are presented for the case of planar impact. Results are then presented and compared for compaction under 1D cylindrically convergent conditions to determine the response predicted, and to determine if these differences could be observed using the PHELIX driver with proton radiography as a diagnostic. Finally, closing remarks are given regarding applicability of the Ramp and P-α compaction models for accurately capturing the dynamic compaction response of porous materials.

2 Compaction Models

Ramp Model

The single-stage Ramp transforms an initially porous material to a state on the EOS using a single linear transformation. For a material starting off at an initial porous density of ρ_{00}, the pressure along the Ramp is defined by:[1]

$$p_1(\rho) = a(\frac{\rho}{\rho_{00}} - 1) \quad , \tag{1}$$

where p_1 is the pressure along the Ramp, ρ is the shock compressed density, and a is the slope of the Ramp. A basic assumption in the single-stage (as well as the bi-linear) Ramp is that the pressure along the Ramp is al-

ways greater than the pressure on the EOS for densities less than that of the theoretical maximum density. This assumption works fine for materials whose Hugoniot response is "normal", but may pose problems for highly porous Hugoniots that exhibit an "anomalous" response. By anomalous, the author is referring to the condition where increases in pressure can result in decreased solid densities. For a more complete description of this behavior, see Ref. [4]. Graphically, the single-stage Ramp is shown by the line p_1 intersecting the "normal" Hugoniot at density ρ_1 in Fig. 1. The intersection of p_1 with the EOS is commonly referred to as the "crush strength" of the material, and represents the pressure at which all of the porosity has been removed from the material.

The bi-linear Ramp uses the same framework as the single-stage Ramp, with the addition of a second linear region:[1]

$$p_2(\rho) = b(\frac{\rho}{\rho_{00}} - c), \tag{2}$$

where b is the slope of Ramp 2, c is a non-dimensional fitting parameter, and the bi-linear compaction behavior is fully defined by Eqns. (1) and (2). For the bi-linear Ramp the compaction response is defined such that the material compresses along p_1 until the condition $p_2 > p_1$ is met, after which it compresses along p_2 until reaching the EOS. This is shown schematically as the solid lines in the compaction region in Fig. 1.

For the Ramp model, release from a pressure state within the compaction region (below the intersection of p_1 or p_2 with the EOS in Fig. 1) is reversible, in that the release behavior is controlled by the slope of the ramp defined by Eqns. (1) and (2). Release from pressures in excess of those needed to intersect the EOS are controlled by the EOS; however, as pressures drop below this intersection release can occur in one of two ways. If 'reversibility' is specified, then the slope of the ramp controls the release behavior, as above. However, if 'irreversibility' is specified, then the slope of the EOS surface continues to define the release path. The default behavior in FLAG is for the Ramp to be 'irreversible'.

The attractiveness of the single-stage and bi-linear Ramp treatments lie in their relative simplicity and flexibility. However, the relative simplicity comes at a cost, as the Ramp models are known to be deficient in their ability to accurately calculate sound speeds and temperatures while the material is in an elevated pressure state on the Ramp. Sound speeds on the Ramp are calculated using the reduced relation:

$$c^2 = \left(\frac{\partial P}{\partial \rho}\right)_S , \tag{3}$$

where c is the sound speed and the subscript S indicates that the partial derivative is taken with respect to constant entropy.

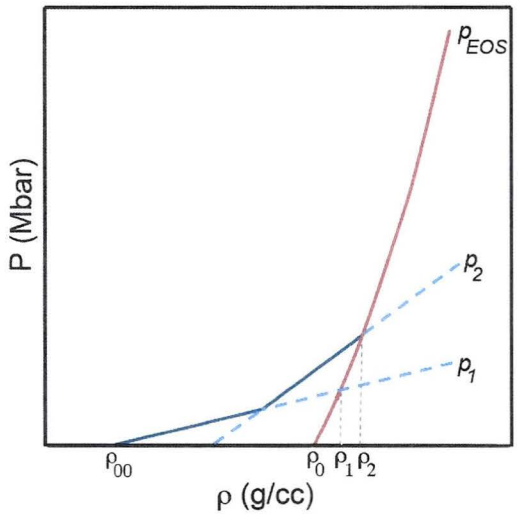

Figure 1: Schematic of general bi-linear Ramp. Image adapted from Ref. [1]

P-α Model

The P-α model has its origins in the late 1960's[5] and early 1970's.[6] In this model, α is a measure of the distention and is described by the relationship $\alpha = V/V_S$, where V is the volume of the porous material, and V_S is the volume of the solid at the same pressure P and temperature T. The parameter α is thus a progress variable toward compaction, such that when $\alpha = 1$ the material is fully solidified and the response is dictated by the EOS. The functional form for $\alpha(P)$ can take many forms, and the specific form investigated in the present work is the two-term (n-term) exponential form captured in the

'pacxp' FLAG model:[1]

$$\alpha(P) = 1 + a_1 exp(-b_1 P) + a_2 exp(-b_2 P). \quad (4)$$

In the preceding equation, a_1, a_2, b_1, and b_2 are fitting parameters where a_x is unitless and b_x has units of inverse pressure (Mbar^{-1}). Equation (4) is shown graphically in Fig. 2 for a generic material that has a crush pressure of approximately 0.15 Mbar. The flexibility of the n-term exponential model, where n = 1, 2, 3, ..., allows a wide array of compaction data to be fit within the constructs of this model. In contrast to the Ramp model, which

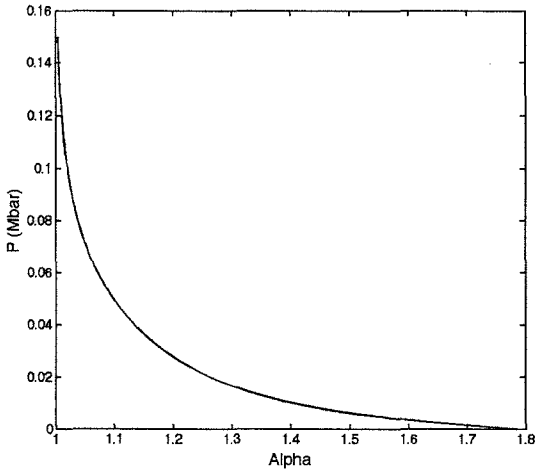

Figure 2: Schematic illustrating $P(\alpha)$ for Eqn. (4).

computes pressure directly from the calculated density through Eqns. (1) and (2), pressure in the P-α model is computed using the relation $P = \alpha^{-1} f(V/\alpha, E)$,[6] which takes into account that pressure acts on both the solid material and the voids. For the P-α model, sound speeds in the porous material are calculated using the standard relation:

$$c^2 = \left(\frac{\partial P}{\partial \rho}\right)_S + \frac{P}{\rho^2}\left(\frac{\partial P}{\partial E}\right)_\rho . \quad (5)$$

Note that the formulations for calculating sound speeds are different between the Ramp and P-α models, Eqns. (3) and (5), where the Ramp model formulation omits the second term because pressure is not a function of energy on the ramp. For Eq. (5) the total energy E includes the compaction energy, or compaction potential. At present this quantity is not well defined, such that some level of uncertainty is introduced with its addition.

Model Fits to CeO_2 Data

A series of dynamic impact experiments have been conducted on several different initial particle morphologies of CeO_2. For these experiments, all morphologies of the CeO_2 were pressed to an approximate initial density of 55% theoretical maximum density (TMD).[7, 8] The experiments were conducted using the planar impact gas-gun facilities at LANL, and were designed specifically to measure the Hugoniot response of CeO_2 both in and above the compaction region. In these experiments, a Cu flyer plate embedded in a sabot (either Al or Lexan) was accelerated toward a stationary target composed of a Cu impactor, the CeO_2 sample, and a PMMA window. The transit time of the shock through the material was measured with a series of velocimetry probes, and the diameters of the targets were designed such that the experiment should remain 1D until after the shock passed through the powder and entered the window. Using the measured shock velocity and initial (pre-shocked) density of CeO_2, along with the measured impact velocity U_D and known Hugoniots of the flyer plate and impactor materials, the Hugoniot state of the CeO_2 was calculated using the method of impedance matching.[7]

The available compaction data for CeO_2 for $P < 0.15$ Mbar were fit to the Ramp model using Eqns. (1) and (2) and to the P-α model using Eqn. (4). The resultant model fits are given in Table 1, and are shown graphically in Fig. 3. From Fig. 3 one observes that both model forms can capture the measured Hugoniot response in the compaction regime quite well, with the P-α model smoothly varying with increasing pressure, and the bi-linear Ramp exhibiting a break in linearity at $P \sim$0.025 Mbar. In both models, the porosity is nearly fully crushed out at pressures between $0.125 \leq P \leq 0.150$ Mbar.

Table 1: Ramp and P-α model parameters for ρ_{00} = 4.03 g/cm^3 CeO_2.

Ramp Model	
a	0.04298
b	0.425
c	1.485
P-α Model	
a_1	0.32499
a_2	0.46813
b_1	162.972
b_2	31.365

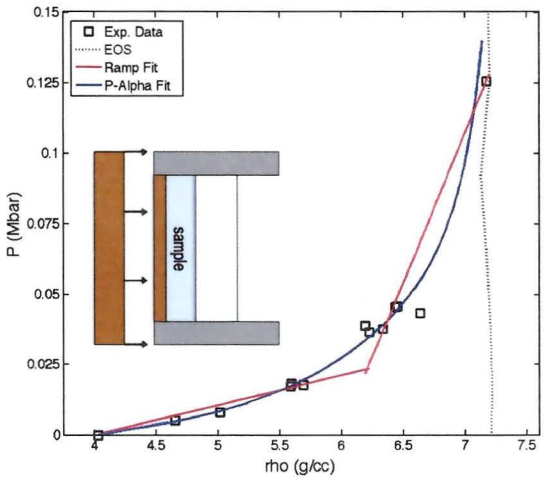

Figure 3: Comparison of Ramp and P-α model fits to CeO_2 data, with schematic of experimental setup.

3 Planar Compaction of CeO_2

Having satisfactorily captured the measured compaction response using the Ramp and P-α compaction models, the model parameters given in Table 1 were used in 1D hydrocode simulations to examine how the Hugoniot response, the shock and release response, and the shock and re-shock response vary as a function of model choice. Calculations were performed using version 3.6.Alpha.20 of FLAG, with a uniform mesh size of 5 μm. For investigation of the Hugoniot and shock and release responses, simulations were setup to replicate three 1D planar impact experiments covering the compaction region, from low pressure (P ~0.017 Mbar, Shot 56-12-01[8]), to intermediate pressure (P ~0.046 Mbar, Shot 1S-1525[8]), to high pressure where the CeO_2 is nearly fully compacted (P ~0.126 Mbar, Shot 2S-589[7]). For the shock and re-shock calculations, the simulations were the same as those described above, with the exception that the low impedance PMMA window was replaced with a higher impedance LiF window. A summary of the relevant materials and material models used in the calculations are given in Table 2. For a more detailed description of the experimental geometries used to setup the simulated geometries, see Fig. 3 and Refs. [7] and [8]. Generally, a thick sabot fronted by a 3 mm flyer plate impacted a 1.5 mm impactor, which was backed by a CeO_2 sample of either 1.5 or 2.0 mm thickness and a window with a thickness of either 14 or 16 mm.

Table 2: SESAME equation of state and FLAG strength models used for the various simulations.

Part	Mat.	EOS	Strength	Refs.
Sabot	Al	3720	PTW	[9]
Sabot	Lexan	7741	ISOCGY	[11]
Flyer	Cu	3336	PTW	[9, 10]
Impactor	Cu	3336	PTW	[9, 10]
Sample	CeO_2	96171	N/A	[12]
Window	PMMA	7741	ISOCGY	[11]
Window	LiF	7271	N/A	

Calculated Hugoniots

The three experiments previously defined were simulated with the Ramp and P-α compaction models defined by Table 1. The calculated Hugoniot was obtained by placing a tracer particle 5 μm into the CeO_2 sample and recording the steady state values achieved for P and ρ. Results from the three sets of calculations are shown schematically in Fig. 4, along with available experimental data and the model fits. Examination of Fig. 4 reveals that both models are able to reproduce the measured Hugoniot of CeO_2 with adequate accuracy at low, intermediate, and high pressures within the compaction regime.

Therefore, if one desires only to accurately simulate the initial Hugoniot response of a material, then both the Ramp and P-α compaction models can be used.

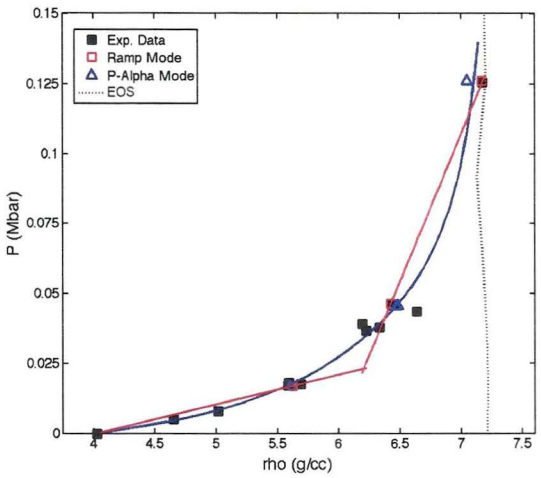

Figure 4: Simulated Hugoinot results for the Ramp and P-α compaction models shown with experimental data and model fits.

Calculated Shock and Release

To examine off-Hugoniot states, and specifically the shock and release response of CeO_2 modeled with the Ramp and P-α compaction models, simulations were again performed for geometries and impact conditions corresponding to experiments 56-12-01, 1S-1525, and 2S-589. These experiments/simulations are considered shock and release in the sense that the unloading wave reflected back into the powder from the window is at a lower pressure than the initial pressure in the powder. The calculated release states can thus be compared directly to experimental results, keeping in mind that at later times experimental results will exhibit two dimensional affects that one dimensional simulations will not.

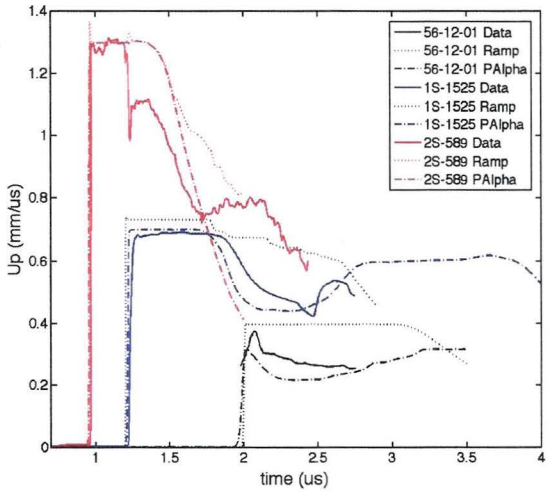

Figure 5: Calculated and experimental results for shock and release response of CeO_2.

The results given in Fig. 5 show that different release behaviors are observed for the compaction models. At the lowest pressures (and material velocities u_p), the geometry of experiment 56-12-01 resulted in release from the rear of the flyer plate at some point inside the powder, prior to the main compaction front reaching the velocimetry surface at the powder/window interface.[8]. Thus, a steady state material velocity was not measured experimentally after shock breakout at the window, but rather a rise and immediate fall in material velocity was measured. Inspection of Fig. 5 reveals that of the two models, the P-α model most closely matches the contoured behavior of u_p, while the Ramp model predicts a steady state material velocity that persists for approximately 1 μs.

At intermediate pressures the two compaction models are more consistent in their relative behavior, and more closely match the initial release response of CeO_2. Comparison of each model with the experimental data reveals that the P-α model performs better at matching the initial equilibrium released state of CeO_2, while the Ramp compaction model predicts a slightly higher material velocity state. Following the initial steady state region, a drop in material velocity corresponding to release from the back surface of the flyer plate is observed. In the experiment and P-α model prediction, the evolution of material velocity can be characterized as relatively smooth and continuous. In contrast, the release behavior for the Ramp model is neither smooth or continuous; rather, it exhibits a jagged response with several distinct changes in slope separating regions of nearly steady state velocity. These observations suggest that both models can more accurately capture the measured release response under steady wave conditions than if the waves are evolving.

For the highest pressures investigated, the experimental results are affected by two dimensional waves relatively soon after initial shock breakout at the window. This is observed as the sharp drop in material velocity that occurs approximately 0.25 μs after shock breakout in the experimental velocity profile. Therefore, only the initial portion of the experimental wave profile can be used in assessing the extent to which either the Ramp or P-α models can capture the measured response. Inspection of Fig. 5 reveals that at pressures where nearly all of the porosity has been crushed out both the Ramp and P-α models predict the equilibrium released state to similar degrees, and both are in satisfactory agreement with the experimental data. It is not until later times, well into the evolution of release, that the two models begin to differ in their behaviors.

Therefore, comparison of the model responses indicates that agreement between the Ramp and P-α compaction models increases with increasing extent of compaction, and that the P-α model captures features of the experimentally measured release states better than the Ramp model, particularly under steady wave conditions.

Calculated Shock and Re-Shock

The shock and re-shock states experienced by CeO_2 as a function of compaction model are shown in Fig. 6. For this impact configuration, corresponding experimental results are not available, such that comparisons can only be made between the two models. At the lowest pressures, the two initial re-shock states differ by 14 m/s, or approximately 7%, where the Ramp model predicts a higher material velocity for the equilibrium re-shock state. However, the structure of the re-shock waves differ significantly between the two models, where the Ramp exhibits a relatively long duration steady state response and the P-α model exhibits an immediate reduction in material velocity followed by a relatively steady region.

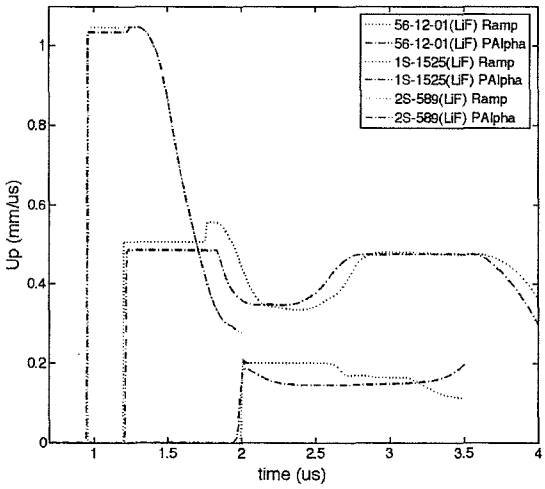

Figure 6: Calculated results for shock and re-shock state of CeO_2.

At intermediate pressures the steady state re-shock state differs by 21 m/s, or approximately 4%, where again the Ramp model predicts the higher material velocity. In this instance, both models predict a steady state re-shock response. However, the Ramp model exhibits a second rise in material velocity at the powder/window interface prior to release from the rear of the flyer plate, while the P-α model does not. Following the initial release region, both wave profiles exhibit similar characteristics, with the major difference being that late-time features for the Ramp model are delayed relative to the P-α model.

At the highest pressures the steady state re-shock state differs by only 12 m/s, or approximately 1%, where the Ramp model predicts slightly higher material velocities.

In opposition to the intermediate pressure case, a second rise in material velocity is observed for the P-α model and not the Ramp model. For the P-α model, the second rise in material velocity achieves the initial material velocity state predicted by the Ramp model and may indicate a state on the EOS where the material is fully consolidated. At later times (corresponding to release from the flyer plate), both the Ramp and P-α models predict similar behaviors, where on the scales of Fig. 6 the two are indistinguishable, again suggesting that at these later times the material response is controlled by the EOS and not the compaction models.

Therefore, comparison of the model responses for the re-shock state indicates that agreement between the Ramp and P-α compaction models increases with increasing extent of compaction, and that the two models vary in predicting a second re-shock state with increasing pressure.

Summary of Planar Results

Given the model fits to experimental data provided in Table 1 and shown in Fig. 3, simulations performed with either the Ramp or the P-α compaction models can adequately reproduce the measured Hugoniot response. It is not until one begins to probe states outside of those for which the models were calibrated, e.g. the shock and release and shock and re-shock states, that one begins to observe differences between the two compaction model implementations. For both the shock and release and shock and re-shock cases, agreement between the two models increased with increasing pressure and extent of compaction. Thus, as one approaches the EOS the two models behave similarly. In instances where extent of compaction is less, the two models vary in their predicted response. In the intermediate compaction regime, the Ramp model tends to predict higher material velocities for both the shock and release and the shock and re-shock cases. For the former, where velocity profiles can be compared to experiments, the P-α model more accurately reflects the general trends measured in the experimental response. In the low pressure compaction regime the Ramp model again predicts higher material velocities for both the release and re-shock conditions. Further, in instances where structure is measured in the transmitted shock and release wave profile, the P-α model is able to capture the general features of the structure, while the Ramp model predicts a nearly steady state material velocity.

Therefore, the Ramp and P-α compaction models exhibit differences in their predicted responses in the one dimensional compaction regime, especially in off-Hugoniot states, and in instances where planar impact data exists, the P-α model more closely reflects the experimental data, with the Ramp model performing the poorest upon release.

4 Cylindrical Compaction of CeO_2

The compaction models defined in Sec. 2 are now applied within cylindrically convergent geometries. One dimensional cylindrically symmetric calculations were performed using FLAG 3.6.Alpha.20, where a schematic of the geometry is given in Fig. 7. In these calculations, the CeO_2 had a radius of 12.7 mm, the initially stationary Al liner had a thickness of 2 mm, and the impacting Al flyer was either 4 or 5 mm thick. A uniform radial mesh dimension of 100 μm was applied to the CeO_2, and the Al mesh size was impedance matched to that of the CeO_2. The material models for CeO_2 and Al were the same as those given in Table 2 with the exception of the Al EOS, which for the cylindrically convergent simulations was SESAME EOS 3717.

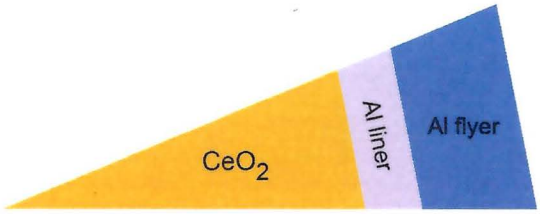

Figure 7: Schematic illustrating geometry of 1D cylindrically converging CeO_2 simulations.

Compaction Physics Calculations

The first set of cylindrical calculations were designed to investigate the behavior of CeO_2 in the porous compaction regime, i.e. at pressures below those required to achieve full densification. To achieve this, a 5 mm

thick Al flyer was impacted against the stationary target (55% TMD CeO_2 and solid Al liner) at a velocity of 1.0 mm/μs. Upon entering the CeO_2 the compaction pressures are equivalent between the Ramp and P-α models. However, as compaction proceeds significant differences are observed.

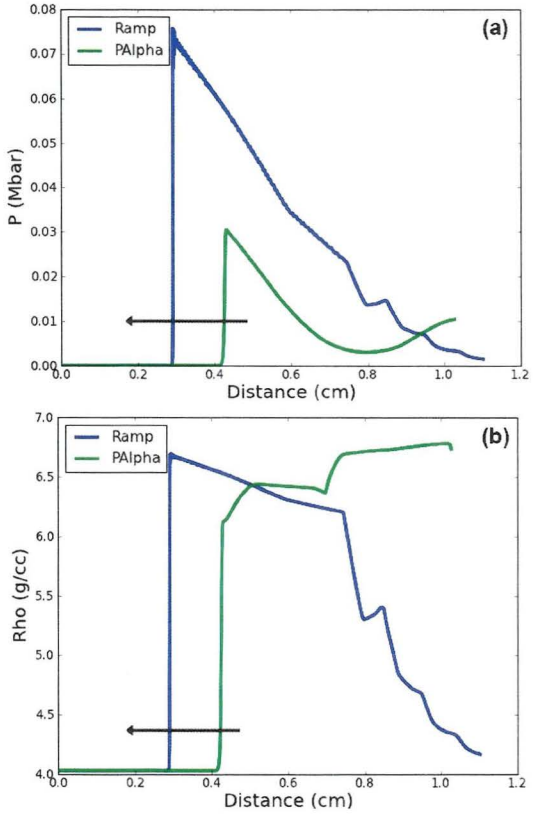

Figure 8: Calculated profiles of (a) pressure and (b) density in the CeO_2 for time t = 5 μs after impact. Arrow indicates direction of wave front propagation.

Figure 8 illustrates the calculated pressure and density profiles in the CeO_2 5 μs after impact of the Al flyer with the Al liner. Here one observes that the initial compaction front for the Ramp has travelled further inward than the P-α model, indicating compaction wave speeds are higher in the Ramp model under cylindrically convergent conditions. Furthermore, inspection of the calculated pressure profiles shows that the peak pressure in the Ramp model is more than twice that of the P-α model at the same instance in time. In addition to differences in shock arrival and peak pressures, Fig. 8 also illustrates that the calculated density states behind the shock front are dissimilar between the two models.

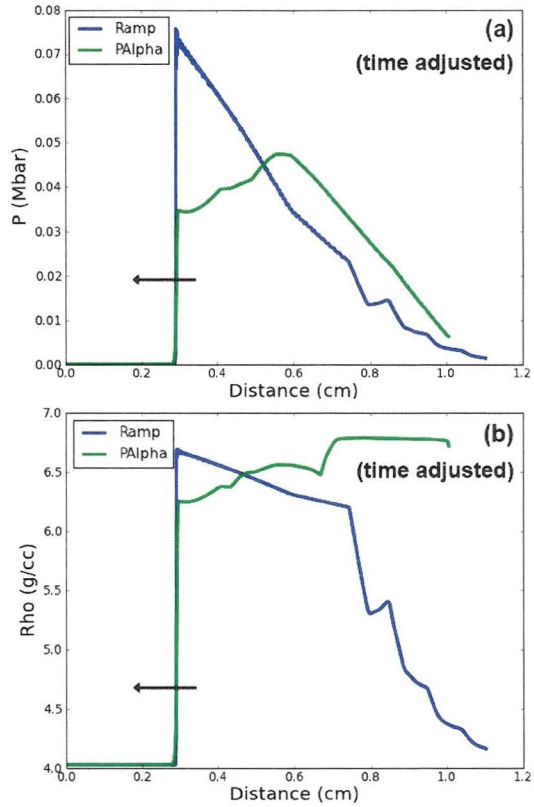

Figure 9: Time-adjusted profiles of the (a) pressure and (b) density in the CeO_2 for t_{Ramp} = 5.0 μs and $t_{P-\alpha}$ = 5.88 illustrating profiles with similar shock breakout locations. Arrow indicates direction of wave front propagation.

To gain further insight into determining how much of the observed variations in pressure and density are due to

convergence (pressures build with convergence) and how much are due to differences in the underlying models, the P-α calculation is advanced in time to t = 5.88 μs such that shock-breakout locations between the two models are coincident. In doing so, the influence of convergence on the calculated responses is minimized, as both models have propagated similar distances into the CeO_2. The resultant, time-adjusted, pressure and density profiles are given in Fig. 9. Inspection of Fig. 9(a) reveals that at comparable levels of convergence the pressure profiles due to model form are significantly different, with the Ramp model exhibiting a sharp peak at shock breakout followed by a continual reduction as pressure is released behind the front. In contrast, the compaction wave produced by the P-α model shows a gradual increase in pressure after shock breakout, followed by a continual reduction of pressure. In both implementations of the models, the pressures near the outer surface of the CeO_2 are low, indicating that nearly full release from the free surface of the Al flyer has occurred.

At similar levels of convergence, calculated density states behind the shock are also quite different between the two models, as shown in Fig. 9(b). Calculated densities immediately following shock breakout are approximately P ~6.66 GPa for the Ramp model and P ~6.24 GPa for the P-α model, a spread of nearly 6% of the theoretical solid density. Differences in characteristics of the density profiles continue with increasing distance from the shock front, as reductions in density are observed from the Ramp model and increases in density are observed from the P-α model. These distinct density profiles, especially those furthest from the shock front (near the outer surface of the CeO_2), are likely due to differences in how release is captured in the two model frameworks. For the Ramp model, the relatively low pressures experienced in the simulation results in a release behavior that occurs along the trajectory of the Ramp. Therefore, as shock pressures are reduced the corresponding released density follows along the Ramp. For the P-α model, release from a partially compacted state occurs at constant porosity, such that as pressure drops the material remains in its partially compacted state, as evidenced by the late time pressure and density profiles in Fig. 9(a) and (b).

Differences in the shocked state are also observed following convergence and reflection of the main compaction front off the central axis. Time-adjusted wave

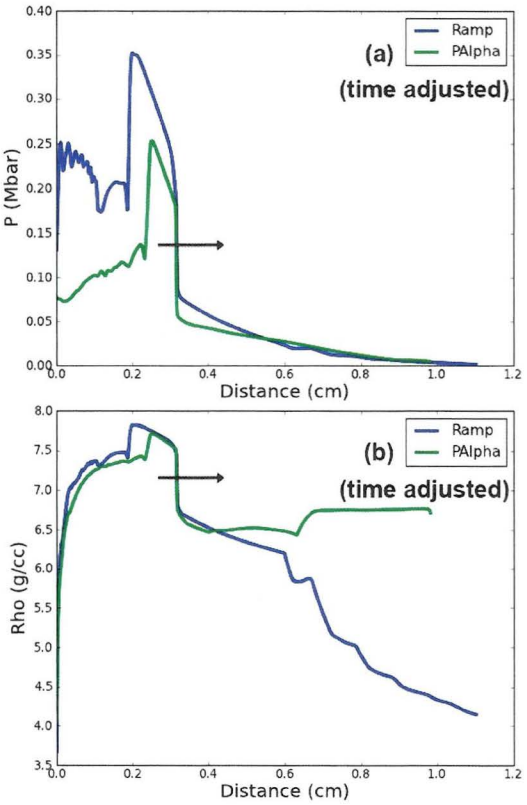

Figure 10: Time-adjusted reflected wave profiles of the (a) pressure and (b) density in the CeO_2 for t_{Ramp} = 6.5 μs and $t_{P-\alpha}$ = 7.75 illustrating similar reflected shock front locations. Arrow indicates direction of wave front propagation.

profiles for the reflected waves are given in Fig. 10, where the P-α simulations are advanced in time to align the reflected wave fronts. Inspection of Fig. 10(a) reveals that significant differences in the high pressure state behind the reflected shock occur as a result of model choice. At similar reflected shock propagation distances the P-α model predicts lower pressures than those from the Ramp, not only in the initial reflected shock, but also along the central axis. Calculated density states behind the reflected shock are more comparable between the two models, as shown in Fig. 10(b), where the largest difference is observed in the width of the high density state immediately behind the reflected shock.

Therefore, at pressures within the compaction regime the Ramp and P-α models calculate significantly different shocked states under cylindrically imploding drive conditions, and while the P-α model captures more of the relevant physics, its performance under cylindrically converging shock waves has not yet been tested.

High-Pressure Physics Calculations

The second set of cylindrical calculations were designed to investigate the behavior of CeO_2 at pressures in excess of those required to achieve full densification. To achieve this drive condition a 4 mm thick Al flyer was impacted against the stationary target (55% TMD CeO_2 and solid Al liner) at a velocity of 2.5 mm/μs. Under these drive conditions the leading shock front exceeds the compaction pressure defined in Table 1 for both the Ramp and P-α models at all times. Representative wave profiles in the CeO_2 during shock convergence are given in Fig. 11, where the two model predictions are observed to be nearly coincident. Both models exhibit a response characterized by a sharp rise in pressure, followed by release. The density profiles exhibit similar features, where full consolidation of the CeO_2 is achieved at the shock front, and behind the front densities are reduced as pressures decrease. While not shown explicitly here, both models also predict consistent responses through convergence and reflection off the central axis at these elevated pressures, suggesting that the equation of state is dominant and that the compaction model has little affect on the the calculated response.

Therefore, at pressures in excess of those required to achieve full densification, good agreement between the Ramp and P-α compaction models occurs, such that either model choice produces similar calculated results.

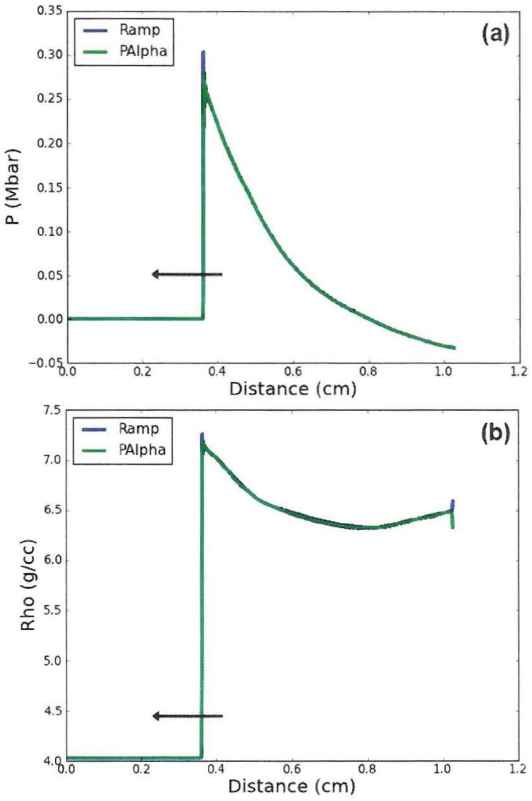

Figure 11: Calculated profiles for the (a) pressure and (b) density in the CeO_2 for time t = 2.5 μs after impact at V_I = 2.5 mm/μs. Arrow indicates direction of wave front propagation.

Summary of Cylindrical Results

Simulations performed under cylindrically convergent drive conditions showed that large differences occur between the Ramp and P-α models when pressures remain below those required to reach full densification. The most marked differences are observed in the compaction wave speeds and in the portions of the wave strongly affected by

release. In the compaction region, the wave speeds predicted by the Ramp model are consistently greater than those from the P-α model, and at any time during convergence results in higher peak pressures for the Ramp model. As distance from the shock front increases, so too do the differences in densities predicted by the two models. The Ramp model releases toward a density corresponding to its initial porous density, while the P-α model remains at elevated densities following the release from high pressure; differences that stem from the methods by which release from a high pressure state are captured by the two models. It is believed that the PHELIX drive platform, coupled with proton radiography, could be used to measure a comparable response experimentally to determine how well either of the computational models perform at capturing the actual response. Above the compaction regime, the two model responses are nearly coincident, indicating that the EOS controls the material behavior.

Therefore, the Ramp and P-α compaction models exhibit significant differences in their predicted responses in the cylindrically convergent compaction regime, with the Ramp model predicting higher wave speeds and initial peak pressures near shock breakout and lower densities following release from the high pressure state.

5 Discussion

The two most widely used compaction models in FLAG are the Ramp model and the P-α compaction model. Results from the present calculations showed that responses predicted between the two models varied widely when pressures remained below those required to achieve full densification. From a practical viewpoint this means that when simulating the shock response of initially porous materials at high pressures, in excess of those needed to achieve full densification, there should be little difference in the calculated results with either the Ramp or P-α compaction model. This indicates that the n-term exponential form of the P-α model used in the present investigation does not explicitly correct for the compaction potential, such that at pressures in excess of the compaction regime the two model implementations are similar.

If pressures are expected to remain relatively low such that the simulated material remains within the compaction regime, then the choice of compaction models is expected to significantly affect the calculated results, particularly for off-Hugoniot states. The fact that both compaction models can reproduce the measured Hugoniot response in the compaction regime under one-dimensional planar impact loading conditions is not surprising, as both models used this data for calibration. This finding simply validates that the models have been formulated such that they can recover the data set for which they were calibrated. Model formulations are not truly stressed until they are exercised outside of the regime in which they have been directly calibrated, such as in off-Hugoniot states. In these regimes the two models were found to predict responses that were quite different from one another.

In the one dimensional planar loading configuration, where data exists for the shock and release response of CeO_2, the P-α model was found to perform better at capturing the initial released state for steady waves (see initial plateau in material velocity profiles for 1S-1525 in Fig. 5). However, as the shock wave becomes unsteady, agreement between the P-α model and the data begins to exhibit more substantial variations. This disagreement is observed in Fig. 5 for both shot 56-12-01, which experienced release from the rear of the flyer in the porous CeO_2 prior to the shock wave reaching the velocimetry surface at the window, and for shot 1S-1525. Consequently, the planar loading calculations suggest that when characteristics of the waves are steady, the P-α model can adequately capture both the Hugoniot and off-Hugoniot released states of a material in the compaction regime, and it is not until the material response evolves along an isentropic release path that calculations begin to substantially diverge from experimental data. To improve agreement of model predictions with experiments in planar off-Hugoniot states, additional experiments to characterize the sound speeds at pressure could be conducted using gas-gun and velocimetry techniques.

In cylindrically convergent geometries the compaction wave is constantly evolving. If one assumes the main compaction front is un-affected by release, then its magnitude increases with propagation distance due to convergence. However, in the geometry simulated in the present work the main compaction front is influenced by both convergence affects and release, resulting in a complex wave structure as the shock approaches, and is reflected off, the central axis. These types of complex wave in-

teractions are expected to stress both the Ramp and P-α compaction models in a regime well outside of where they have been calibrated, and in a regime where they have yet to be validated. The authors believe that the PHELIX platform, coupled with proton radiography, could be used to help determine how well the Ramp and P-α compaction models perform under complex loading configurations.

If high levels of confidence are required for simulations employing either the Ramp or P-α compaction models in a regime where complex wave interactions are expected, and the magnitude of those waves are such that the material remains within the compaction regime, then further validation of these models should be conducted.

6 Summary

Calculations were performed by employing both the Ramp and P-α compaction models for planar and cylindrically driven shock loading geometries. Both models were able to reproduce the experimentally determined Hugoniot response under steady planar loading conditions, the conditions under which the models were calibrated. However, in off-Hugoniot states, and especially in states where complex wave interactions occur, calculated responses for the two models diverge from one another and from experiment, such that further validation of the models under complex loading conditions is recommended. For 1D planar loading, sound speed at pressure measurements would be useful in constraining model behavior. For non-planar complex loading, cylindrically convergent compaction experiments conducted on PHELIX, using proton radiography to track the shock front and density distribution behind the shock, could be used to help further constrain model behavior.

References

[1] J.L. Hill, *(U) Users Manual for FLAG version 3.6.0*, LANL Report, LA-CP-17-20057 (2017).

[2] Y. Horie, A.B. Sawaoka, *Shock Compression Chemistry of Materials*, (KTK Scientific Publishers: Tokyo), 1991, Ch. 4.

[3] W.A. Reass, D.M. Baca, J.R. Griego, R.E. Reinovsky, C.L. Rousculp, P.J. Turchi, *Precision High Energy Liner Implosion Experiments PHELIX*, LANL Report, LA-UR-09-05309 (2009).

[4] Y.B. Zel'dovich, Y.P. Raizer, *Physics of Shock Waves and High-Temperature Hydrodynamic Phenomena*, (New York: Dover Publications Inc.), 2002 pp. 712-716.

[5] W. Herrmann, J. Appl. Phys. **40** (1969) 2490-2499.

[6] M. Carroll, A.C. Holt, J. Appl. Phys. **43** (1972) 759-761.

[7] D.A. Fredenburg, D.D. Koller, P.A. Rigg, R.J. Scharff, *Rev. Sci. Instrum.* **84**, 013903 (2013).

[8] D.A. Fredenburg, D.D. Koller, J.D. Coe, C.B. Kiyanda, *J. Appl. Phys.* **115**, 123511 (2014).

[9] S.-R. Chen, G.T. Gray III, *Summary of the PTW Model Parameters*, LANL Report, LA-UR-04-0920 (2004).

[10] D.L. Preston, D.L. Tonks, D.C. Wallace, *J. Appl. Phys.* **93**, (2003) 211-220.

[11] Z. Rosenberg, in *Shock Waves in Condensed Matter - 1983*, (Amsterdam: Elsevier Science Publishers), 1984, pp. 247-249.

[12] E.D. Chisolm, *SESAME 96171, a three-phase equation of state for CeO_2*, LANL Report, LA-UR-12-25524 (2012).